Topologically Protected All-Optical Memory

Seou Choi, Jungmin Kim, Jeonghun Kwak, Namkyoo Park,* and Sunkyu Yu*

The in-memory processor has played an essential role in overcoming the von Neumann bottleneck, which arises from the partition of memory and a processing unit. Although photonic technologies have recently attracted attention for ultrafast and power-efficient in-memory computing, the realization of an all-optical in-memory processor remains a challenge. This difficulty originates from the contradiction between robustness and sensitivity in wave dynamics, requiring both noise-immune memory states and modulation-sensitive transitions between these states. Here, a building block that provides an all-optical transition between topologically protected memory states is proposed. A nonlinear photonic molecule that satisfies parity-time (PT) symmetry, revealing multiple oscillation quenching states with different degeneracies determined by PT-symmetric phases is investigated. In terms of topology for dynamical systems, these quenching states support topologically protected dynamical trajectories suitable for stable memory states. An all-optical bidirectional transition between these states, which allows incoherent memory switching is demonstrated. The result provides design criteria for all-optical in-memory processors with multilevel operations, enabling the classical-wave counterpart of electronic memristors.

1. Introduction

The well-known "memory wall bottleneck,"[1] which originates from the separation of processing and storage units in von Neumann architecture, has renewed the necessity of realizing memory functions near signal processors. The expected solution for overcoming this bottleneck includes near- or in-memory computing,[2] which imposes memory functions on processing units or vice versa. A representative example is found in electronics: the memristor, which is the so-called missing fourth circuit element.[3,4] The nonvolatile analog memory functions incorporated with Ohm's law and Kirchhoff's law in an electronic memristor enable in-memory signal processing for artificial neural networks.[5] On the other hand, the realization of an in-memory processing unit in integrated photonics is not yet successful, especially for all-optical devices, although some insightful memory-related applications have been demonstrated such as stopping light,[6] electro-optical quantum memristors,[7] flip-flop memory,[8] and all-optical integrators.[9]

To realize a photonic in-memory processor, its unit element must satisfy the following design criteria: multiple error-robust optical memory states and efficient transitions between them. First, the unit element needs to support optical states that are robust to possible noise or defects in its operation to stably memorize the state of light. Second, similar to a one-transistor–one-memristor (1T1R) configuration in electronics,[5] the unit element should include a toolkit for bidirectional transitions between multiple memory states. Notably, these criteria should be satisfied with a platform that is integratable with all-optical signal processors, for example, allowing state-preserving readout of the memory states. However, these criteria—the robustness of optical states to possible defects and the energy-efficient tunability—are usually contradictory, as proven in topological[10] and disordered photonics[11] and sensing applications.[12] The design of a photonic memristor-analogous unit for in-memory processors is thus not a straightforward task.

In this paper, we propose an all-optical building block for photonic in-memory processors by exploiting dynamical parity-time (PT)-symmetric systems. We classify PT-symmetric phases and analyze the Lyapunov stability[13] for a triatomic PT-symmetric system including saturable nonlinearities. The analysis shows the coexistence of topologically protected stable states, that is, oscillation quenching states. We also demonstrate that the building block allows incoherent switching between these oscillation quenching states through all-optical modulations. With the simultaneous achievement of topology-enabled error robustness and all-optical transition in a platform integratable with all-optical signal processors, our study will pave the way for realizing robust photonic in-memory processors.

S. Choi, J. Kim, S. Yu
Intelligent Wave Systems Laboratory
Department of Electrical and Computer Engineering
Seoul National University
Seoul 08826, Korea
E-mail: sunkyu.yu@snu.ac.kr
S. Choi, J. Kim, N. Park
Photonic Systems Laboratory
Department of Electrical and Computer Engineering
Seoul National University
Seoul 08826, Korea
E-mail: nkpark@snu.ac.kr
J. Kwak
Department of Electrical and Computer Engineering
Inter-University Semiconductor Research Center
Seoul National University
Seoul 08826, Korea

**ADVANCED
SCIENCE NEWS**

www.advancedsciencenews.com

**ADVANCED
ELECTRONIC
MATERIALS**

www.advelectronicmat.de

2. Model Definition

In photonics and general wave mechanics, the terminology "topology" has usually described the topological aspect of a wavefunction in a dispersion band,[10,14,15] which can be quantified by discretized topological invariants such as Chern numbers. However, because the concept of topology—the invariant properties of a geometrical object under arbitrary continuous deformations—is universal, topological properties and their related phenomena can be defined for any form of a geometric object that allows continuous deformation. Therefore, the concept of topology has been applied to other wave quantities rather than wavefunctions in reciprocal space, such as the geometrical nature of Fermi surfaces, where the topological invariant is defined by the disconnection of isofrequency surfaces.[16] In handling dynamical systems, we focus on the topological properties of the "trajectories" of optical states, which have been widely employed in dynamical theory.[13] In previous works on non-Hermitian and nonlinear photonic molecules,[17,18] we demonstrated the topological classification of the dynamical trajectories of optical "intensity" distributions, also showing the critical role of PT symmetry in the form of the dynamical trajectories. Because of the nature of topology, the deliberate design of the photonic molecules allows for the existence of topologically protected stable states—oscillation quenching states[17,18]—which preserve their convergent dynamical trajectories, and therefore, provide subsequent noise immunity. The previous works also provided the extension of traditional PT-symmetric systems composed of gain and loss elements[19] into dynamical systems accessed by optical nonlinearity, also generalizing the underlying physics from the static phase transition across the exceptional point[20] to the PT-symmetry-dependent oscillation quenching states.

Although such topologically protected quenching states provide robustness to any type of defect as long as the defect preserves dynamical trajectories, the oscillation quenching states in previous platforms[17,18] cannot provide the all-optical memory functions necessary for in-memory processors. It is due to the lack of coexisting multiple stable states—at least ON and OFF states are necessary for binary-level memory, which

should also be tunable with all-optical modulation. Therefore, the previous approaches can be applied only to single-channel applications or externally modulated multichannel devices such as laser stabilization, signal regeneration, or electro-optical rectification.[17,18]

To realize multiple oscillation quenching states in a given system and achieve an all-optical transition between these states, we investigate a triatomic PT-symmetric photonic molecule composed of one Hermitian and linear resonator and two non-Hermitian and nonlinear resonators (**Figure 1**). In the linear regime, the triatomic PT-symmetric system has been widely studied to utilize higher-order exceptional points (EPs)[12,21–25] for enhanced sensitivity,[12] mechanical cooling,[21] cavity magnonics systems,[23] successive state conversion,[24] and wireless power transfer.[22,25] To extend the higher-order EP system into memory functions, we employ the emergence of oscillation quenching states and the transition between them, realizing binary (ON–OFF) stable states (Figure 1). We emphasize that the application of nonlinear PT-symmetric systems to photonic memory is also in accordance with the necessity of open systems for memorizing wave states because the combination of unitary operations in closed systems is insufficient to describe non-Markovian processes.[7]

The proposed molecule for multiple quenching states consists of gain and loss resonators that are mutually connected through the neutral (gainless and lossless) resonator. The gain and loss resonators possess saturable nonlinearity in their amplification[26] and dissipation,[27] respectively. The time-varying light fields in this system are then modeled by temporal coupled-mode theory (TCMT) as follows:[28]

$$\frac{d}{dt}\begin{bmatrix} \psi_G \\ \psi_N \\ \psi_L \end{bmatrix} = i\begin{bmatrix} \omega_0 - i\gamma_G & \kappa & 0 \\ \kappa & \omega_0 & \kappa \\ 0 & \kappa & \omega_0 + i\gamma_L \end{bmatrix}\begin{bmatrix} \psi_G \\ \psi_N \\ \psi_L \end{bmatrix} \qquad (1)$$

where $\psi_{G,N,L}$ are the field amplitudes inside gain (G-), neutral (N-), and loss (L-) resonators, respectively; $\gamma_{G,L} = \gamma_{G0,L0}/(1 + |\psi_{G,L}/\psi_{GS,LS}|^2)$ are the saturable gain and loss coefficients, respectively, for the linear coefficients $\gamma_{G0,L0} \geq 0$ and the
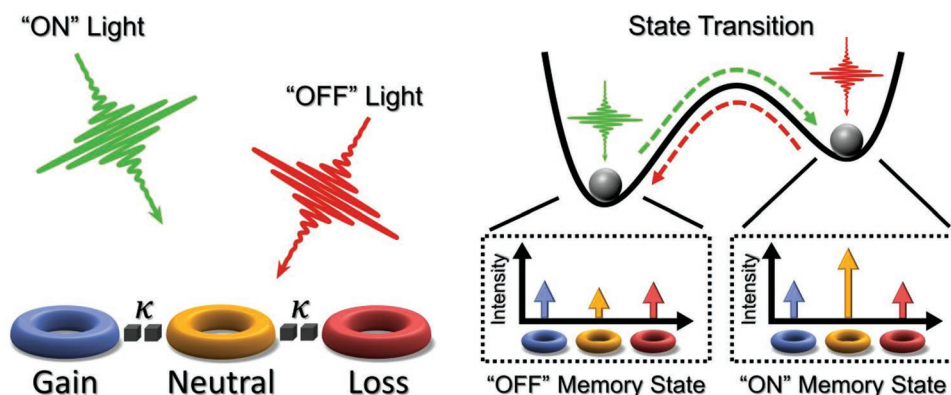
Figure 1. All-optical memory using oscillation quenching states. The schematic figure illustrates the operation principle of the proposed all-optical memory system. The system consists of a neutral (gainless and lossless) resonator coupled with nonlinear gain and loss resonators through the coupling coefficient κ. The suggested platform supports the coexistence of binary (ON–OFF) stable states, which have different optical intensity distributions inside the platform. "ON" (green) and "OFF" (red) light signals lead to the bidirectional transition between these stable states.

saturation intensities $I_{GS,LS} = |\psi_{GS,LS}|^2$; ω_0 is the resonant frequency; and κ is the coupling coefficient. While such saturable nonlinearities can be achieved with conventional optical gain and saturable absorbers, the intensity-dependent nonlinearities of the gain and loss resonators dynamically alter the phase of PT symmetry, depending on the field energy accumulated inside each resonator.

Although Equation (1) cannot be described by explicit solutions, the harmonic approximation ($\partial_t \psi_{G,N,L} \sim i\omega\psi_{G,N,L}$) provides useful insight into the understanding of the PT-symmetric phase in the system. The eigenvalue analysis with the harmonic approximation (Note S1, Supporting Information) then leads to the indicators $c_\pm$ for PT-symmetric phases:

$$c_+ = \frac{\beta}{\sqrt[3]{\delta + \sqrt{-\beta^3 + \delta^2}}}, c_- = \sqrt[3]{\delta + \sqrt{-\beta^3 + \delta^2}} \tag{2}$$

where β and δ are dynamical coefficients as functions of the system ($\gamma_{G0,L0}$, $\psi_{GS,LS}$, ω_0, κ) and wave ($\psi_{G,L}$) parameters, as follows:

$$\beta = \left(\frac{\gamma_L - \gamma_G}{3}\right)^2 + \frac{\gamma_G\gamma_L}{3} - \frac{2\kappa^2}{3},$$
$$\delta = -\frac{\gamma_L - \gamma_G}{3}\left\{\left(\frac{\gamma_L - \gamma_G}{3}\right)^2 + \frac{\gamma_G\gamma_L}{2} + \frac{\kappa^2}{2}\right\} \tag{3}$$

We restrict our discussion in the regime of $\beta < 0$, guaranteeing $c_+ < 0$ and $c_- > 0$, and therefore, enable the explicit description of PT-symmetric phase transition (see Note S1, Supporting Information). The PT-symmetric phases of the system are then classified with the eigenfrequencies ω_{1-3} in the harmonic approximation: i) unbroken PT-symmetric phases satisfying Im[ω_{1-3}] = 0 with $|c_+| = |c_-|$ and ii) broken PT-symmetric phases satisfying Im[ω_1] $\neq$ Im[$\omega_{2,3}$] with $|c_+| \neq |c_-|$. From $c_+ = \beta/c_-$ with Equation (2) and the definition of δ with Equation (3), the condition for unbroken PT symmetry $|c_+| = |c_-|$ is identical to $\delta = 0$ or $\gamma_G = \gamma_L$.

3. Coexisting Oscillation Quenching

To explore the oscillation quenching states that result in stable field intensities inside resonators,[17,18] we examine the dynamics of the real-valued field intensities $I_{G,N,L}$ obtained from the separation of amplitudes and phases in the complex-valued field $\psi_{G,N,L} = (I_{G,N,L})^{1/2}\exp(i\theta_{G,N,L})$.[29] Notably, because the applied optical nonlinearities in Equation (1) are dependent only on the field intensity, the equation for $I_{G,N,L}$ describes well the stability and transition condition of optical states, as described in later sections.

To independently analyze $I_{G,N,L}$ from the nonlinear equations in Equation (1), which has six degrees of freedom ($I_{G,N,L}$ and $\theta_{G,N,L}$), it is necessary to remove the degrees of freedom on optical phases $\theta_{G,N,L}$. Neglecting the global phase, we try to characterize the possible values of the phase differences $\theta_{rs} = \theta_r - \theta_s$ (r, s = {G, N, L}) by examining the eigenmodes of the system under the harmonic approximation (Note S2,

Supporting Information). As examined in Note S2, Supporting Information, the unbroken or broken phase of PT symmetry determines such phase differences between resonator fields θ_{rs}, leading to analytically solvable differential equations for $I_{G,N,L}$. With some straightforward algebra (Note S2, Supporting Information), we classify three dynamical phases with different equilibria: the "U$_1$" and "U$_2$" phases with unbroken PT symmetry and the "BR" phase with broken PT symmetry, which are analytically derived from $\partial_t I_{G,N,L} = 0$ at ω_1 (U$_1$ phase) and $\omega_{2,3}$ (U$_2$ and BR phases).

For simplicity, we introduce real-valued parameters: $\gamma = \gamma_{L0}/\gamma_{G0}$, $\chi = I_{LS}/I_{GS}$, $\kappa_r = \kappa/\gamma_{G0}$, $p = [(\gamma\chi - 1)^2 + 4\chi\kappa_r^2]^{1/2}$, and $q = \gamma\chi - 1$. The nontrivial equilibria ($I_{G,N,L} \neq 0$) of the U$_{1,2}$ and BR phases, which are solely determined by the system parameters, are then obtained as follows (Note S2, Supporting Information):

$$I_{G,U1} = I_{L,U1} = I_U = \frac{1-\gamma}{\chi\gamma - 1}I_{LS}, I_{N,U1} = \left[\frac{\gamma\chi - 1}{(1-\chi)\kappa_r}\right]^2 I_U \tag{U1, 4}$$

$$I_{G,U2} = I_{L,U2} = I_U = \frac{1-\gamma}{\chi\gamma - 1}I_{LS}, I_{N,U2} = 2I_U \tag{U2, 5}$$

$$I_{G,BR} = \frac{1}{\chi}\left(\frac{2}{p-q} - 1\right)I_{LS},$$
$$I_{L,BR} = \left(\frac{2\gamma\chi}{p+q} - 1\right)I_{LS}, \quad I_{N,BR} = I_{G,BR}\left[\frac{(p-q)^2}{4\kappa_r^2} + 1\right] \tag{BR, 6}$$

With some tedious but straightforward algebra, we demonstrate the stability conditions of those nontrivial equilibria by using the first Lyapunov criterion[13] (see Notes S3–S5, Supporting Information, for details). This analysis shows that the U$_1$ and U$_2$ phases correspond to a twofold degenerate oscillation death (OD),[30] satisfying partially inhomogeneous steady states (IHSS) of $I_G = I_L \neq I_N$. In contrast, the BR phase leads to a nondegenerate OD, resulting in complete IHSS of $I_G \neq I_L$, $I_G \neq I_N$, and $I_L \neq I_N$. Because these equilibria are also hyperbolic equilibria that do not have Jacobian eigenvalues on the imaginary axis, it is critical to note that the phase portraits of the system near the equilibria of the U$_{1,2}$ and BR phases are locally topologically equivalent to those of its linearized system according to the Grobman–Hartman theorem.[13] This topological nature of the dynamical trajectories in the U$_{1,2}$ and BR phases, therefore, guarantees the "protection" of the stable dynamics.

To achieve switchable memory states, the system requires the coexistence of stable phases. **Figure 2**a shows the phase diagram of stable equilibria as a function of two system parameters χ and γ. The diagram represents the coexistence regions of the stable phases among the U$_1$ (Figure 2b), U$_2$ (Figure 2c), and BR phases (Figure 2d), which are characterized by the analysis in Notes S3–S6, Supporting Information. In Figure 2a–d, we reveal two coexisting phases: i) the C$_{U1-U2}$ phase, where two unbroken (U$_{1,2}$) PT-symmetric phases coexist, and ii) the C$_{U1-BR}$ phase, where unbroken (U$_1$) and broken (BR) PT-symmetric phases coexist. Notably, we analytically examine the phase
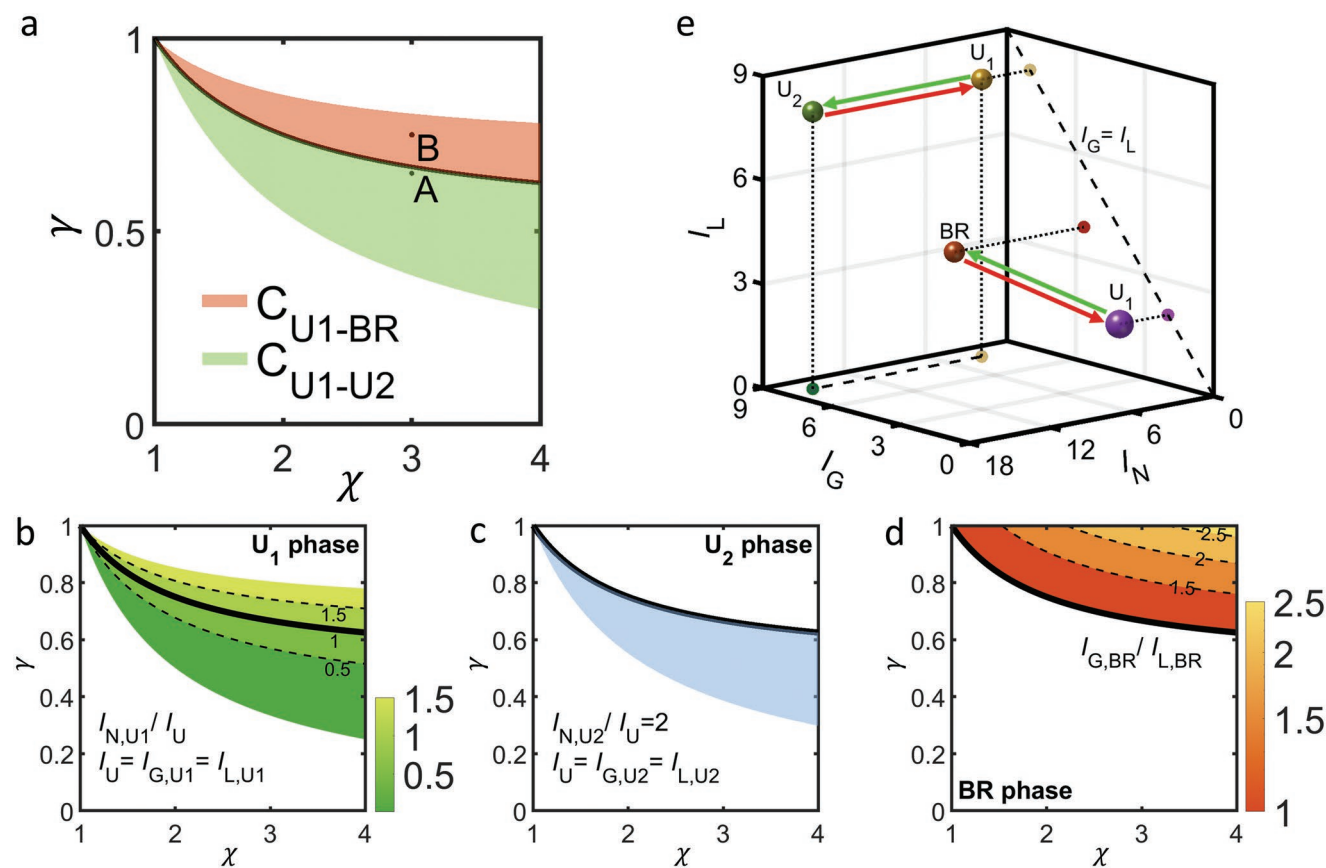
Figure 2. Phase diagrams of oscillation-quenching states for all-optical memory. a) Coexisting phase diagram obtained from individual phase diagrams of the stable b) U_1, c) U_2, and d) BR phases defined in the γ–χ plane. Green and red areas in (a) represent two coexisting phases, the $C_{U1\text{-}U2}$ and $C_{U1\text{-}BR}$ phases, respectively. The $C_{U1\text{-}U2}$ phase supports the coexistence of U_1 and U_2 stable phases, while the $C_{U1\text{-}BR}$ phase supports the coexistence of U_1 and BR stable phases. The colored regions in (b–d) show the ratios of (b) $I_{N,U1}/I_U$, (c) $I_{N,U2}/I_U = 2$, and (d) $I_{G,BR}/I_{L,BR}$. e) The design strategy of the all-optical binary memory function. The phase diagram in (a) provides the allowed ranges of γ and χ for binary memory states, which are defined in the I_G-I_N-I_L parameter space according to the results in (b–d). The all-optical modulation alters the intensity distribution inside the photonic molecule, achieving an all-optical transition between the memory states in the same coexisting phase (green and red arrows). $\gamma_{G0} = 0.005$, $\kappa_r = 0.5$, and $I_{GS} = 4$ for all cases.

boundary between the $C_{U1\text{-}U2}$ and $C_{U1\text{-}BR}$ phases (see Note S6, Supporting Information) as:

$$\gamma = \kappa_r + \frac{1-\kappa_r}{\chi} \qquad (7)$$

This phase boundary corresponds to the amplitude death (AD) state satisfying the threefold degeneracy $I_G = I_L = I_N$ of the homogeneous steady state (HSS) in the U_1 phase.[30] At the same time, the boundary denotes the PT-symmetric phase transition between U_2 and BR phases, which composes the "dynamical exceptional line" in the parameter space $\gamma\chi$, as the dynamical counterpart of the exceptional point in static systems.[20,31] We also emphasize that the coexisting phases $C_{U1\text{-}U2}$ and $C_{U1\text{-}BR}$ inherently include two stable states at a given set of system parameters, in sharp contrast to previous approaches that support only a unique stable state with the fixed PT-symmetric phase.[17,18]

For a given set of system parameters, each coexisting phase supports multiple stable equilibria, which are protected by the topology of the state trajectories in the wave quantity space: the 3D parameter space of I_G-I_N-I_L. Therefore, we can envisage

the realization of robust all-optical memory by using these equilibria as "topologically protected memory states". The all-optical transition between these memory states (Figure 2e) can then be achieved by altering the intensity distribution inside a system, as discussed later.

The analysis in Figure 2 and Notes S1–S6, Supporting Information, employs the harmonic approximation and stability theory near the equilibria. To confirm the validity of our approach, we conduct a time-domain analysis of our nonlinear governing equation, Equation (1), by applying the sixth-order Runge–Kutta method.[32] While the complete analysis requires 5D data for the initial conditions (I_G ($t = 0$), I_N ($t = 0$), I_L ($t = 0$), $\angle\psi_G - \angle\psi_N$, $\angle\psi_L - \angle\psi_N$), we focus on the "2D-projected" view (I_G, I_N) on dynamic trajectories for a clear visualization by fixing the initial I_L and $\angle\psi_{G,N,L}$. **Figure 3** shows the results of this analysis for the different coexisting phases of $C_{U1\text{-}U2}$ (point "A" in Figure 2a) and $C_{U1\text{-}BR}$ (point "B" in Figure 2a). As demonstrated, we observe the coexistence of different oscillation quenching states obtained from Figure 2. Although these states are topologically protected, as shown in the convergence of nearby initial states, the clear boundaries in Figure 3 imply that the alteration in the I_G-I_N plane will lead to the transition
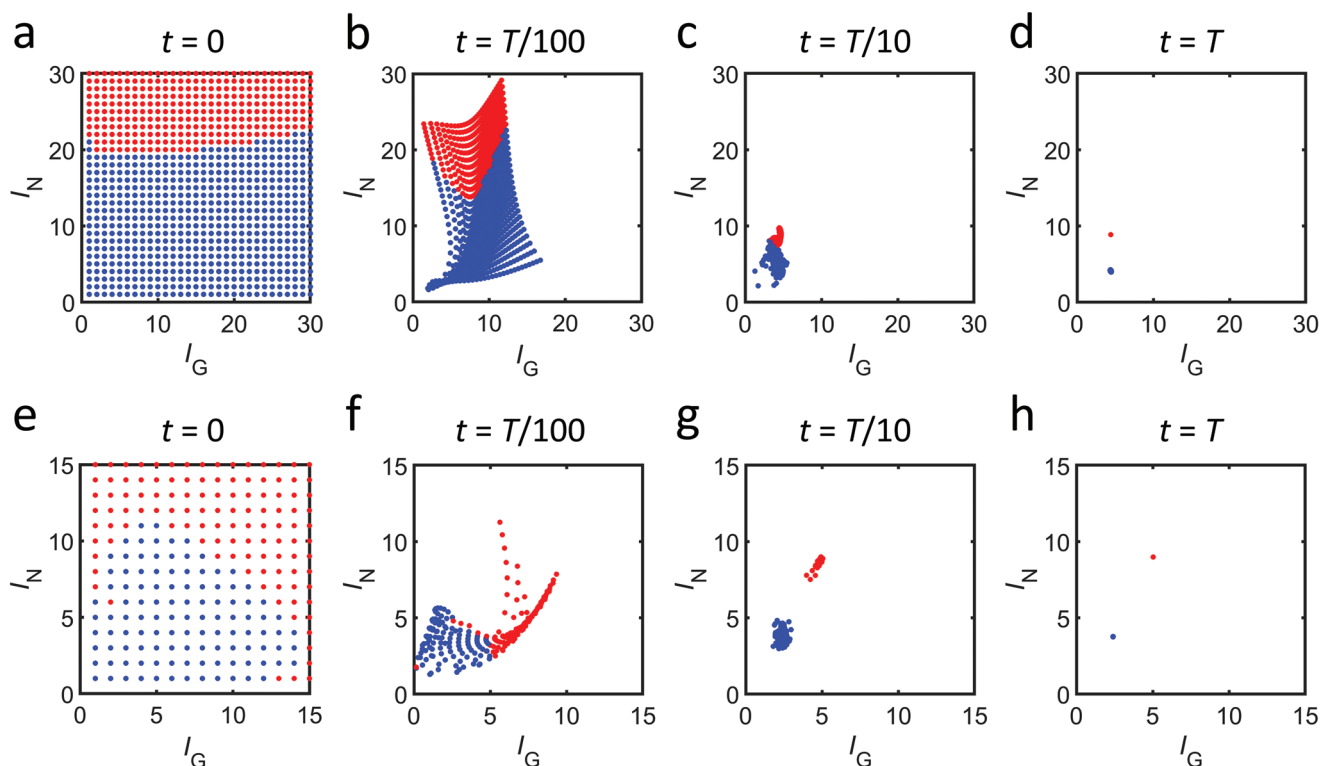
Figure 3. Topological protection of oscillation quenching states. Projected dynamical state trajectories of the a–d) C_{U1-U2} phase and e–h) C_{U1-BR} phase on the I_G-I_N plane. a,e) Blue and red circles represent the initial states that will converge to (a) U_1 and U_2 phases at point A in Figure 2a, respectively, and (e) U_1 and BR phases at point B in Figure 2a, respectively. (b–d) and (f–h) describe the time evolutions from (a) and (e), respectively. The simulation time is $T = 2 \times 10^5/\omega_0$. Dynamical evolutions are calculated by the sixth-order Runge–Kutta method with a unit step of $2\pi/(200\omega_0)$ and the initial condition $I_L = 5$, $\angle\psi_G = 0°$, $\angle\psi_N = 90°$, and $\angle\psi_L = 135°$. See Movies S1 and S2, Supporting Information, for the temporal evolutions of (a–d) and (e–h), respectively.

between different oscillation quenching states. The time-domain analysis also provides the convergence time for each stable state (see Note S7, Supporting Information). Notably, this characteristic time corresponds to the erase/write times of this photonic memory and is much longer in more degenerate cases (the U_1 and U_2 phases compared to the BR phase, Figure S3 in Note S7, Supporting Information), emphasizing the role of PT symmetry in the operation speed of the all-optical memory.
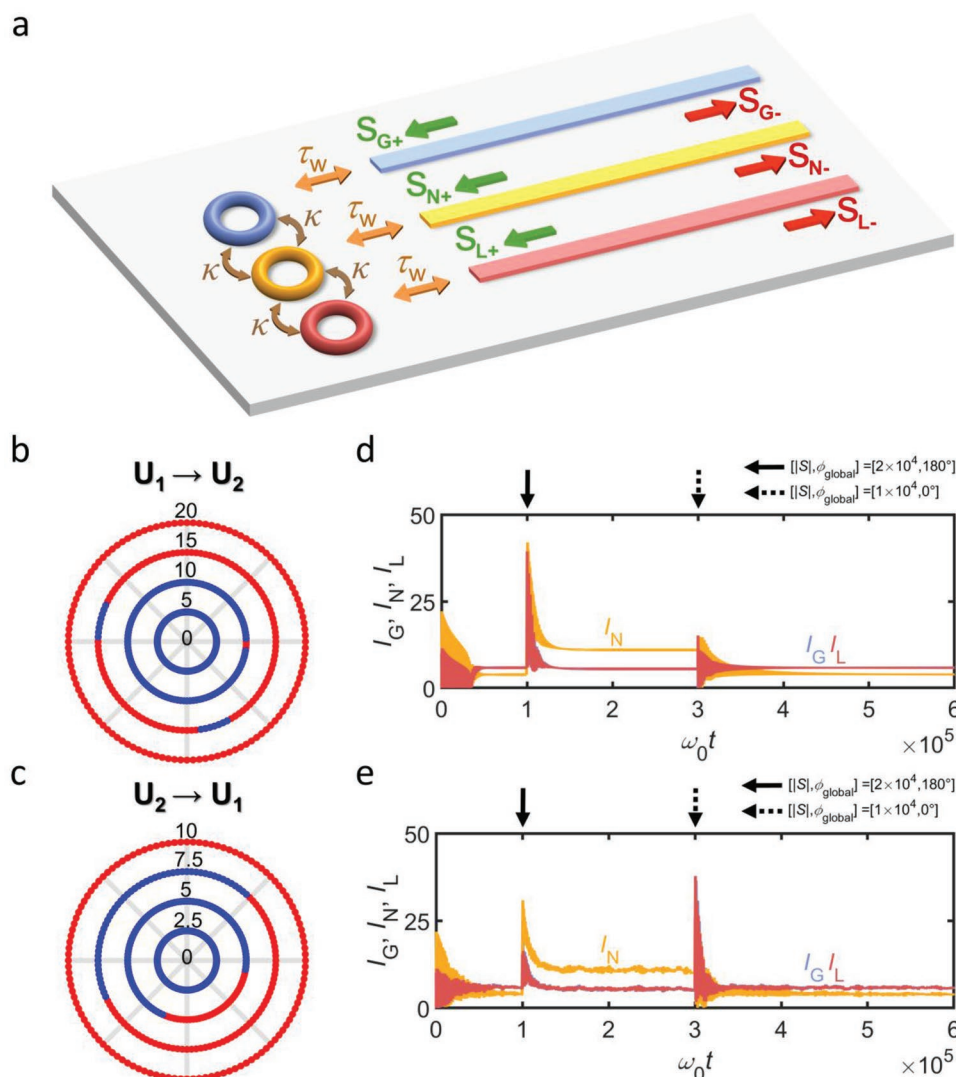
4. All-Optical Transition

In addition to the stability of each memory state, we now focus on the all-optical transition between memory states. To demonstrate the transition, we include the modulating waveguides evanescently coupled to the photonic memory platform (**Figure 4**a), which is again examined by the TCMT equation and its numerical analysis (see Note S8, Supporting Information). Due to the weak coupling between waveguides and resonators, these waveguides allow state-preserving readout of the memory states inside resonators through the outgoing waves $S_{G-,N-,L-}$, which constitute the platform integratable with all-optical signal processors.

The modulation light exerted on each resonator is defined by three complex fields $S_{G+,N+,L+} = |S|\exp(i\varphi_{\text{global}})S_{G,N,L}$, which include wave degrees of freedom in the global intensity ($|S|$),

global phase (φ_{global}), and local complex fields $S_{G,N,L}$. The phase and amplitude of local complex fields $S_{G,N,L}$ can be manipulated with integrated photonic elements,[33] and the global intensity $|S|$ directly corresponds to the modulation power. Therefore, for the practical implementation of all-optical memory, the critical issue is to realize modulation, that is, insensitive to the global phase φ_{global} because it is difficult to access the relative phase difference between φ_{global} and the optical phase inside resonators.

Figure 4b,c show the "incoherent"—φ_{global}-independent—bidirectional transition between the stable U_1 phase and the stable U_2 phase, achieved with delta-function modulation. We set $S_{G,N,L}$ for each transition according to the post-transition state of the local complex fields inside resonators. We then examine the emergence of the transition as a function of $|S|$ and φ_{global}. As demonstrated, we observe the ranges of $|S|$ for both $U_1 \rightarrow U_2$ and $U_2 \rightarrow U_1$ transitions, which allow incoherent state transitions between memory states. Based on these results, we show the all-optical transition between memory states with time-domain simulations (Figure 4d). Memory states are clearly distinguished by $I_{N,U1}$ and $I_{N,U2}$, indicating the "low" (or OFF) and "high" (or ON) levels in a binary memory cell. The emergence of the peaks at $\omega_0 t \approx 1 \times 10^5$ and $\omega_0 t \approx 3 \times 10^5$ represents the dynamical trajectories from the transition between memory states (red and blue dots in Figure 3d), which will be affected by both $|S|$ and φ_{global}.

**ADVANCED
SCIENCE NEWS**
www.advancedsciencenews.com

**ADVANCED
ELECTRONIC
MATERIALS**
www.advelectronicmat.de

Figure 4. All-optical transition between noise-immune binary memory states. a) A schematic diagram of all-optical photonic memory with the read–write waveguide paths, supporting the incoming modulation signals $S_{G+,N+,L+}$ and the outgoing signals $S_{G-,N-,L-}$. The waveguides are weakly coupled to each resonator with the lifetime τ_w. Unidirectional transition map (red: transition, blue: no transition) for b) $U_1 \rightarrow U_2$ and c) $U_2 \rightarrow U_1$. Radial and polar axes indicate $|S| \times 10^{-3}$ and φ_{global}, respectively. $S_{G,N,L}$ are determined by the target equilibria defined in Notes S3 and S4, Supporting Information. Time-domain analysis of the all-optical transition between binary memory states: d) without and e) with optical noise. The solid and dashed arrows in (d,e) denote the exertion of the transition signal. In (e), the uniformly random noise of the amplitude $u(0, 5)$ and phase $u(-\pi, \pi)$ for each time step are additionally applied to $S_{G+,N+,L+}$. $\gamma_{G0} = 0.005$, $l_{GS} = 4$, $\chi = 2$, $\gamma = 0.7$, $\kappa_r = 0.5$, and $\tau_w = 2 \times 10^5$. The Runge–Kutta method in Figure 3 is employed.

Figure 4b,c, therefore, verify that our design realizes the transition between "coherent memory states" (between the resonators, which are protected by eigenmodes) through the "incoherent modulation" (between the incident and memory fields). Such a property demonstrates a critical advantage of the proposed platform because it is notoriously difficult to detect the phase information of the memorized optical state. Our theory based on the intensity-dependent dynamical equations allows the binary switching of the memorized eigenmodes through the modulation signal with arbitrary phases regardless of the time-varying phase of the memorized light states.

To clarify the noise immunity originating from the topological protection of each memory state, we also investigate the

all-optical transition against the random noise in the modulation signal. For complete randomness, we assume the noise in both the amplitude and phase of the modulation signal. The uniformly random noise signal $S_{noise,X} = u[0,5]\exp(iu[0,2\pi])$ is imposed on the ideal modulation signal, where $u[a,b]$ denotes the random distribution between a and b and the symbol X = G, N, and L depicts a specific resonator of the system. Even with such a noise signal independently applied to each resonator, the proposed platform realizes φ_{global}-independent switching, which allows the practical incoherent erase/write operation of photonic memory (Figure 4e, see also Note S9, Supporting Information, for all-optical transitions between the U_1 and BR phases).

2200579 (6 of 9)

5. Practical Implementation

Due to the platform transparency of our TCMT, which describes nonlinear optical dynamics with dimensionless parameters and abstract geometry, the obtained results in Figures 2–4 are valid for any frequency bands (radio frequency, terahertz, infrared, etc.), resonant structures (RLC circuits, microdisks, metamaterials, etc.), and wave mechanics (photonics, acoustics, etc.) when suitable nonlinear gain and loss elements exist. The structural platform for the coupling of gain, neutral, and loss resonators has been widely studied in previous literature on PT-symmetric photonics.[34,35] When considering the cutting-edge technologies in integrated photonics,[34,35] the possible number of memory elements would be $\approx 10^2$–10^3 at this stage, which may be an acceptable number for the application to optical neural networks.[33]

On the other hand, as shown in Figure 2a, the critical parameters in the practical implementation are not the specific values of material parameters, but the "ratios" between them: the ratios ($\gamma = \gamma_{L0}/\gamma_{G0}$, $\chi = I_{LS}/I_{GS}$, $\kappa_r = \kappa/\gamma_{G0}$) among linear gain and loss coefficients (γ_{G0} and γ_{L0}), saturation intensities for amplification and dissipation (I_{GS} and I_{LS}), and coupling coefficient (κ).

In Figures 2–4, we achieve topologically protected all-optical memory in the parameter space of $\gamma < 1$ and $\chi > 1$ with the fixed value of $\kappa_r = 0.5$. Because the coupling coefficient is tunable with the geometric conditions (resonator shapes and spatial distances), the key to the practical implementation is the restriction on gain and loss materials: $\gamma < 1$ (or $\gamma_{L0} < \gamma_{G0}$) and $\chi > 1$ (or $I_{LS} > I_{GS}$). This restriction requires the use of a saturable absorber with a small absorption coefficient and large saturation intensity or a lasing platform with a large amplification coefficient and small saturation intensity. Although various pairs of gain and loss materials can satisfy such conditions in different frequency bands, in this section, we focus on the frequency range near the telecom wavelength (≈ 1550 nm) and assume the conventional Er^{3+}-doped silica amplifying platform. In this three-level lasing system, the rate equation shows that the linear gain coefficient γ_{G0} and saturation intensity I_{GS} are determined by the spontaneous emission lifetime and transition cross-section,[36] doping concentration,[37] and pumping rate.[38] Widely used parameters allow for $\gamma_{G0} \approx 0.1$ GHz and $I_{GS} \approx 0.4$ GW cm^{-2},[36–38] while γ_{G0} and I_{GS} can be manipulated with the pump power (Figure S5a in Note S10, Supporting Information).

Owing to recent attention on achieving nonlinear optical functionalities, such as activation functions for optical neural networks,[33,39] the realization of saturable absorbers with low saturation intensity I_{LS} has been intensively studied. Among many possible candidates for the conditions $\gamma < 1$ and $\chi > 1$, such as single-wall nanotubes,[40] graphene,[41] topological insulators,[42] and MoS_2,[43] we assume the doping or deposition of a ZnO material[44] to lossless resonators. By controlling the modal cross-section to the saturable absorber, γ_{L0} and I_{LS} can be controlled near the values of γ_{G0} and I_{GS}, respectively. In Figure S5b in Note S10, Supporting Information, an example of practically accessible states in Figure 2a is described with conventional material parameters for gain[36–38] and loss[44] materials. In this scenario, the operation optical intensity is in the range of ≈ 0.1–1 GW cm^{-2}, which requires a few watts of operation power. Because the only energy consumption while maintaining the memory states in our device is the pumping energy to the gain resonator, the value ≈ 0.1–1 GW cm^{-2} directly determines the energy consumption of our optical memory. Such an operation power can be dramatically reduced by introducing artificial saturable absorbers with the Kerr effect,[45] graphene platforms,[41] and metamaterials with phase change materials[46] or plasmonic nonlinearity.[47]

As demonstrated in electronic memory devices, the speed of the memory is estimated by the read/write time.[48] As shown in Figure 4a, our design of all-optical memory is based on the weak coupling of optical waveguides to the resonators, which allows the consistent reading of the current memory states through S_{G-}, S_{N-}, and S_{L-}. Therefore, the read time of the proposed all-optical memory platform is not restricted by the platform itself but will be determined by the connection to external devices, which may be restricted by the speed of optical switching devices supporting the ranges of 10 GHz–1 THz.[49,50]

On the other hand, the write time of our all-optical in-memory processors depends on two mechanisms: i) the convergence time of dynamical state trajectories to stable states and ii) the time duration of the modulation signal necessary for phase transitions between memory states. We note that the speed of both mechanisms depends on the efficiency of the energy exchange between resonators, which is determined by the coupling coefficient κ. For the applied value of κ, we achieve $\approx 10^5/\omega_0$ for the write time, which allows the $\approx$ GHz operation speed for the telecom wavelength (≈ 1550 nm). An order of magnitude increase in the operation speed (>10 GHz) can be achieved when we consider a small value of κ in the current design.

6. Conclusion

In conclusion, we studied the realization of photonic memory platforms that allow all-optical transitions between oscillation quenching states. By applying stability theory and time-domain analysis, we demonstrated that each oscillation quenching state possesses defect robustness, originating from the topological protection of dynamical state trajectories. The coexistence of multiple oscillation quenching states, which have different degeneracies of optical intensity levels (nondegenerate/two-fold ODs and threefold AD), enables the all-optical transition of these robust memory states, achieving seemingly contradictory criteria—robustness and tunability—for memory devices. Because different oscillation quenching states originate from the classification of PT-symmetric phases, our result emphasizes the critical role of non-Hermitian degrees of freedom in dynamical systems.

The observed all-optical dynamics can be generally extended to impose noise immunity on various signal processors including optical switching,[51] logic gates,[52] and memristic weight elements for all-optical neural networks.[53] Although we employed a triatomic system to realize an all-optical in-memory processor, the necessity of multiple memory states in artificial neural networks suggests the importance of examining the higher-order coexistence of oscillation quenching states by

increasing the number of system elements. In handling multiple memory states, the expected hurdle is on achieving analytical solutions for the equilibria and their stability analysis. The possible approach may be found in deep learning,[54,55] which allows for exploring extended design space in nonlinear problems. When considering the result in Figure 3, the coexistence of multiple stable equilibria requires the increased partitioning of the parameter space, while maintaining the noise immunity in each subspace. For determining the optimized number of system elements in the building block for all-optical neural networks, the following study on the transition sensitivity and operation speed for all-optical memory will also be necessary.

Our "classical wave" memory has a clear difference from "quantum" memory,[56,57] which has attracted significant attention in quantum communications. First, our design using the eigenmodes of coupled resonators provides the memory of classical light in terms of two sets of optical quantities: the intensity distribution $I_{G,N,L}$ and the optical coherence inside the memory $\theta_G - \theta_N$ and $\theta_L - \theta_N$. Such quantities can be understood as the "macroscopic" scale observation of quantum probability density and coherence, lacking the memory of single-photon information. On the other hand, classical memory does not suffer from the quantum decoherence issue, as demonstrated in the robustness of state convergence and transition to local and global decoherence of optical states. Because the topological properties are maintained under the continuous deformation of the system and the memory states are defined with the eigenmodes of coupled resonators, our memory system keeps the optical memory states as long as the topological phase transition does not occur. Furthermore, because the levels of memory states are determined by the platform parameters, not by optical signals, the individual states will be stable under large-scale circuit realization. The only requirement for our system is consistent pumping to maintain the gain parameters γ_{G0} and ψ_{GS}. Therefore, our classical wave memory should have differentiated applications from quantum memory, such as classical photonic neural networks, when we consider the critical roles of memristors in electronic neural networks.[5]

Supporting Information

Supporting Information is available from the Wiley Online Library or from the author.

Conflict of Interest

The authors declare no conflict of interest.

Data Availability Statement

All the data used in this analysis are available from the corresponding author upon request.

[1] N. Mahapatra, B. Venkatrao, *Crossroads* **1999**, *5*, 2.
[2] M. Gokhale, B. Holmes, K. Iobst, *Computer* **1995**, *28*, 23.
[3] D. B. Strukov, G. S. Snider, D. R. Stewart, R. S. Williams, *Nature* **2008**, *453*, 80.
[4] L. Chua, *IEEE Trans. Circuit Theory* **1971**, *18*, 507.
[5] P. Yao, H. Wu, B. Gao, J. Tang, Q. Zhang, W. Zhang, J. J. Yang, H. Qian, *Nature* **2020**, *577*, 641.
[6] M. F. Yanik, S. Fan, *Phys. Rev. Lett.* **2004**, *92*, 083901.
[7] M. Spagnolo, J. Morris, S. Piacentini, M. Antesberger, F. Massa, A. Crespi, F. Ceccarelli, R. Osellame, P. Walther, *Nat. Photonics* **2022**, *16*, 318.
[8] L. Liu, R. Kumar, K. Huybrechts, T. Spuesens, G. Roelkens, E.-J. Geluk, T. de Vries, P. Regreny, D. Van Thourhout, R. Baets, G. Morthier, *Nat. Photonics* **2010**, *4*, 182.
[9] M. Ferrera, Y. Park, L. Razzari, B. E. Little, S. T. Chu, R. Morandotti, D. J. Moss, J. Azaña, *Nat. Commun.* **2010**, *1*, 29.
[10] T. Ozawa, H. M. Price, A. Amo, N. Goldman, M. Hafezi, L. Lu, M. C. Rechtsman, D. Schuster, J. Simon, O. Zilberberg, I. Carusotto, *Rev. Mod. Phys.* **2019**, *91*, 015006.
[11] S. Yu, C. Qiu, Y. Chong, S. Torquato, N. Park, *Nat. Rev. Mater.* **2021**, *6*, 226.
[12] H. Hodaei, A. U. Hassan, S. Wittek, H. Garcia-Gracia, R. El-Ganainy, D. N. Christodoulides, M. Khajavikhan, *Nature* **2017**, *548*, 187.
[13] Y. A. Kuznetsov, *Elements of Applied Bifurcation Theory*, Vol. 112, Springer Science & Business Media, Springer, Berlin, Germany **2013**.
[14] L. Lu, J. D. Joannopoulos, M. Soljačić, *Nat. Photonics* **2014**, *8*, 821.
[15] M. Kim, Z. Jacob, J. Rho, *Light: Sci. Appl.* **2020**, *9*, 130.
[16] N. S. K. Harish, Z. Jacob, E. Narimanov, I. Kretzschmar, M. M. Vinod, *Science* **2012**, *336*, 205.
[17] S. Yu, X. Piao, N. Park, *Adv. Sci.* **2019**, *6*, 1900771.
[18] S. Yu, X. Piao, N. Park, *Nanophotonics* **2021**, *10*, 2883.
[19] L. Feng, R. El-Ganainy, L. Ge, *Nat. Photonics* **2017**, *11*, 752.
[20] M.-A. Miri, A. Alù, *Science* **2019**, *363*, eaar7709.
[21] H. Jing, S. K. Ozdemir, H. Lu, F. Nori, *Sci. Rep.* **2017**, *7*, 3386.
[22] M. Sakhdari, M. Hajizadegan, P.-Y. Chen, *Phys. Rev. Res.* **2020**, *2*, 013152.
[23] G.-Q. Zhang, J. Q. You, *Phys. Rev. B* **2019**, *99*, 054404.
[24] A. Laha, D. Beniwal, S. Dey, A. Biswas, S. Ghosh, *Phys. Rev. A* **2020**, *101*, 063829.
[25] M. Sakhdari, M. Hajizadegan, Q. Zhong, D. N. Christodoulides, R. El-Ganainy, P. Y. Chen, *Phys. Rev. Lett.* **2019**, *123*, 193901.
[26] L. Chang, X. Jiang, S. Hua, C. Yang, J. Wen, L. Jiang, G. Li, G. Wang, M. Xiao, *Nat. Photonics* **2014**, *8*, 524.
[27] E. Spiller, *J. Appl. Phys.* **1972**, *43*, 1673.
[28] H. A. Haus, *Waves and Fields in Optoelectronics*, Vol. 464, Prentice-Hall, Englewood Cliffs, New Jersey **1984**.
[29] S. Yu, X. Piao, N. Park, *Phys. Rev. Lett.* **2018**, *120*, 193902.

[30] A. Koseska, E. Volkov, J. Kurths, *Phys. Rep.* **2013**, *531*, 173.

[31] C. E. Rüter, K. G. Makris, R. El-Ganainy, D. N. Christodoulides, M. Segev, D. Kip, *Nat. Phys.* **2010**, *6*, 192.

[32] J. C. Butcher, *J. Aust. Math. Soc.* **1964**, *4*, 179.

[33] Y. Shen, N. C. Harris, S. Skirlo, M. Prabhu, T. Baehr-Jones, M. Hochberg, X. Sun, S. Zhao, H. Larochelle, D. Englund, M. Soljačić, *Nat. Photonics* **2017**, *11*, 441.

[34] M. C. Rechtsman, J. M. Zeuner, Y. Plotnik, Y. Lumer, D. Podolsky, F. Dreisow, S. Nolte, M. Segev, A. Szameit, *Nature* **2013**, *496*, 196.

[35] J. Sun, E. Timurdogan, A. Yaacobi, E. S. Hosseini, M. R. Watts, *Nature* **2013**, *493*, 195.

[36] B. E. A. Saleh, *Fundamentals of Photonics*, Vol. *2*, Wiley Interscience, Wiley, Hoboken, NJ **2007**.

[37] K. Y. Ko, M. S. Demokan, H. Y. Tam, *IEEE Photon. Technol. Lett.* **1994**, *6*, 1436.

[38] L. Qian, *Advanced Labs for Special Topics in Photonics (ECE 1640H)*, University of Toronto, Canada **1998**, pp. 1–36.

[39] B. J. Shastri, A. N. Tait, T. Ferreira de Lima, W. H. P. Pernice, H. Bhaskaran, C. D. Wright, P. R. Prucnal, *Nat. Photonics* **2021**, *15*, 102.

[40] S. Y. Set, H. Yaguchi, Y. Tanaka, M. Jablonski, *J. Light. Technol.* **2004**, *22*, 51.

[41] Q. Bao, H. Zhang, Z. Ni, Y. Wang, L. Polavarapu, Z. Shen, Q.-H. Xu, D. Tang, K. P. Loh, *Nano Res.* **2011**, *4*, 297.

[42] C. Zhao, H. Zhang, X. Qi, Y. Chen, Z. Wang, S. Wen, D. Tang, *Appl. Phys. Lett.* **2012**, *101*, 211106.

[43] H. Ahmad, M. A. Ismail, M. Suthaskumar, Z. C. Tiu, S. W. Harun, M. Z. Zulkifli, S. Samikannu, S. Sivaraj, *Laser Phys. Lett.* **2016**, *13*, 035103.

[44] P. Loiko, T. Bora, J. M. Serres, H. Yu, M. Aguiló, F. Díaz, U. Griebner, V. Petrov, X. Mateos, J. Dutta, *Beilstein J. Nanotechnol.* **2018**, *9*, 2730.

[45] M. Teimourpour, A. Rahman, K. Srinivasan, R. El-Ganainy, *Phys. Rev. Appl.* **2017**, *7*, 014015.

[46] G. Dayal, S. A. Ramakrishna, *Opt. Lett.* **2013**, *38*, 272.

[47] J. Wang, A. Coillet, O. Demichel, Z. Wang, D. Rego, A. Bouhelier, P. Grelu, B. Cluzel, *Light: Sci. Appl.* **2020**, *9*, 50.

[48] C. Busche, L. Vilà-Nadal, J. Yan, H. N. Miras, D.-L. Long, V. P. Georgiev, A. Asenov, R. H. Pedersen, N. Gadegaard, M. M. Mirza, D. J. Paul, J. M. Poblet, L. Cronin, *Nature* **2014**, *515*, 545.

[49] M. Ono, M. Hata, M. Tsunekawa, K. Nozaki, H. Sumikura, H. Chiba, M. Notomi, *Nat. Photonics* **2020**, *14*, 37.

[50] A. Liu, L. Liao, D. Rubin, H. Nguyen, B. Ciftcioglu, Y. Chetrit, N. Izhaky, M. Paniccia, *Opt. Express* **2007**, *15*, 660.

[51] K. Nozaki, T. Tanabe, A. Shinya, S. Matsuo, T. Sato, H. Taniyama, M. Notomi, *Nat. Photonics* **2010**, *4*, 477.

[52] K. K. Mehta, C. Zhang, M. Malinowski, T.-L. Nguyen, M. Stadler, J. P. Home, *Nature* **2020**, *586*, 533.

[53] E. Goi, Q. Zhang, X. Chen, H. Luan, M. Gu, *PhotoniX* **2020**, *1*, 3.

[54] W. Ma, Z. Liu, Z. A. Kudyshev, A. Boltasseva, W. Cai, Y. Liu, *Nat. Photonics* **2021**, *15*, 77.

[55] Q. Wang, L. Zhang, *Nat. Commun.* **2021**, *12*, 1.

[56] T.-S. Yang, Z.-Q. Zhou, Y.-L. Hua, X. Liu, Z.-F. Li, P.-Y. Li, Y. Ma, C. Liu, P.-J. Liang, X. Li, Y.-X. Xiao, J. Hu, C.-F. Li, G.-C. Guo, *Nat. Commun.* **2018**, *9*, 3407.

[57] Y. Ma, Y.-Z. Ma, Z.-Q. Zhou, C.-F. Li, G.-C. Guo, *Nat. Commun.* **2021**, *12*, 2381.